



HAL
open science

Hidden surface channel in two-dimensional multilayers

Youkyung Seo, Soo Yeon Kim, Yeeun Kim, Chulmin Kim, Byung Chul Lee, Yoon Hee Park, Minji Chae, Youjin Hong, Min Kyung Seong, Changhyun Ko, et al.

► **To cite this version:**

Youkyung Seo, Soo Yeon Kim, Yeeun Kim, Chulmin Kim, Byung Chul Lee, et al.. Hidden surface channel in two-dimensional multilayers. *2D Materials*, 2022, 9 (3), pp.035004. 10.1088/2053-1583/ac6343 . hal-03666461

HAL Id: hal-03666461

<https://hal.science/hal-03666461>

Submitted on 15 Nov 2022

HAL is a multi-disciplinary open access archive for the deposit and dissemination of scientific research documents, whether they are published or not. The documents may come from teaching and research institutions in France or abroad, or from public or private research centers.

L'archive ouverte pluridisciplinaire **HAL**, est destinée au dépôt et à la diffusion de documents scientifiques de niveau recherche, publiés ou non, émanant des établissements d'enseignement et de recherche français ou étrangers, des laboratoires publics ou privés.

1 **Hidden Surface Channel in Two-dimensional** 2 **Multilayers**

3 *Youkyung Seo^{§,†,#}, Soo Yeon Kim^{§,†,#}, Yeeun Kim^{†,‡}, Chulmin Kim^{||}, Byung Chul Lee^{||}, Yoon Hee*
4 *Park[§], Minji Chae[§], Youjin Hong[§], Min Kyung Seong[§], Changhyun Ko^{†,§,‡}, Alessandro Cresti^Δ,*
5 *Christoforos Theodorou^Δ, Gyu Tae Kim^{||}, and Min-Kyu Joo^{†,§,‡,*}*

6 [§]Department of Applied Physics, Sookmyung Women's University, Seoul 04310, Republic of
7 Korea

8 [†]Department of Physics, Sookmyung Women's University, Seoul 04310, Republic of Korea

9 [‡]Department of Physics and Astronomy, Seoul National University, Seoul 08826, Republic of
10 Korea

11 ^{||}School of Electrical Engineering, Korea University, 145 Anam-ro, Seongbuk-gu, Seoul
12 02841, Republic of Korea

13 [‡]Institute of Advanced Materials and Systems, Sookmyung Women's University, Seoul 04310,
14 Republic of Korea

15 ^ΔUniv. Grenoble Alpes, Univ. Savoie Mont Blanc, CNRS, Grenoble INP, IMEP-LAHC, 38000
16 Grenoble, France

17

18 *E-mail: mkjoo@sookmyung.ac.kr

19 [#]These authors contributed equally to this work.

20

21 **KEYWORDS:** two-dimensional materials, multilayers, carrier transport, surface doping,
22 interlayer resistance

23

1 **Abstract:** Numerous carrier scatterers, such as atomic defects, fixed oxide charges,
2 impurities, chemical residues, and undesired surface adsorbates, including oxygen and water
3 molecules, strongly degrade the carrier mobility of atomically thin two-dimensional (2D)
4 materials. However, the effect of surface adsorbates and surface oxidation on the carrier density
5 profile along the thickness of 2D multilayers is not well known, particularly for a substantial
6 interruption in the formation of the top-surface channel. Here, we uncover a hidden surface
7 channel in *p*-type black phosphorus and *n*-type rhenium disulfide multilayers originating from
8 undesired ambient adsorbates and surface oxides that not only populate hole density (or reduce
9 electron density) but also suppress carrier mobility. The absence of a second peak in the
10 transconductance curve under ambient conditions indicates the disappearance of the top-
11 surface channel inside the 2D multilayers, which is a possible indicator for the cleanliness of
12 the top surface and can be used in gas sensor applications. Moreover, the negligible variation
13 in the drain bias polarity-dependent turn-on voltage for the bottom channel under ambient
14 conditions validates the exclusive contribution of surface adsorbates to the formation of the top
15 channel in 2D multilayers. Our results provide a novel insight into the distinct carrier transport
16 in 2D optoelectronic devices and diverse sensors.

17

1 1. Introduction

2 Atomically thin two-dimensional (2D) materials, such as graphene, black phosphorus (BP),
3 and transition-metal dichalcogenides (TMDs), have demonstrated unique low-dimensional
4 physical properties with chemically inert surfaces (without out-of-plane dangling bonds), such
5 as quantum phase transition [1], Coulomb drag [2], exciton condensation [3], quantum
6 interference [4], and quantum spin Hall effect [5]. However, these novel 2D physical properties
7 are often hampered and even distorted by various Coulomb impurities, such as atomic defects,
8 fixed oxide charges, impurities, chemical residues, and undesired surface adsorbates, including
9 oxygen and water molecules [6–10], resulting in undesired excess carrier doping [11], surface
10 oxidation [12], and mobility degradation [13,14]. In addition to these vulnerabilities of 2D
11 monolayers, theoretical studies have predicted that the effective mass increases as the number
12 of layers decreases in most 2D materials [15], leading to a relatively low intrinsic carrier
13 mobility in 2D monolayers. This phenomenon limits their various pragmatic applications
14 compared with their multilayer counterparts.

15 2D multilayers, which consist of multiple monolayers, not only exhibit a higher carrier
16 mobility but also demonstrate a better immunity to surrounding Coulomb scatterers than those
17 of monolayers [14,16,17]. These merits render them promising candidates for low-power, low-
18 noise, and high-energy-efficient electronic devices and multifunctional sensors [18].
19 Nonetheless, unlike a monolayer platform, the interlayer resistance (R_{Int}) and the Thomas-
20 Fermi charge screening length strongly influence on the carrier density profile along the c -axis
21 of 2D multilayers and the layer-dependent in-plane carrier mobility, which makes this
22 multilayer system have complex carrier transport mechanism [19]. For example, when the
23 carrier density populates inside 2D multilayers with increasing gate potential at a given R_{Int} ,

1 the layer demonstrating the highest conductivity in the layers shifts from bottom- to top-surface
2 in a conventional back-gate configuration due to the interplaying between R_{Int} and the layer-
3 dependent in-plane carrier mobility [19]. Similarly, a variation of drain bias and temperature
4 could alter the amplitude of R_{Int} , resulting in a change of carrier density profile inside 2D
5 multilayers and leading to exhibit two humps in its corresponding transconductance curve (g_m)
6 [20]. It is worth to note that one prevailing assumption in such a scenario is that carrier mobility
7 corresponding to top-surface channel is always higher than that of bottom-channel mainly
8 because of the enhanced Coulomb scattering effects stemming from an underlying dielectric
9 substrate [11]. On the contrary, when the carrier mobility corresponding to top-surface channel
10 is degraded by undesired surface adsorbates including oxygen and water molecules and
11 structural atomic defects during device fabrication or surface oxidation, the carrier transport
12 via top-surface channel is significantly restricted. This suggests that the presence of top-surface
13 channel can be a possible indicator for the cleanness of top-surface of 2D multilayers.
14 Nevertheless, the importance implication of the shape of transconductance is rarely explored
15 in 2D optoelectronic devices. For instance, since the photocurrent (I_{PH}) strongly relies on
16 carrier mobility ($I_{\text{PH}} \propto \mu \propto g_m$), thereby g_m simply guides us how to maximize I_{PH} and
17 photoresponsivity ($R = I_{\text{PH}}/P \propto g_m$, where P denote the laser power) [21,22].

18 Thus far, numerous 2D van der Waals (vdW) materials have been reported with interesting
19 optoelectronic properties mainly originating from their atomically thin nature (Nat. Rev. Mater.
20 2, 17033 (2017)). Among them, a black phosphorus (BP) multilayer is known to be extremely
21 sensitive to ambient conditions, whereas a rhenium disulfide (ReS_2) is relatively very stable
22 comparing to BP. This contrasting feature makes them ideal platform to study the effects of
23 surface adsorbates and surface oxidation on top of 2D materials. Moreover, an ambipolar BP

1 is an attractive material for future electronics which provides a chance to observe both n - and
2 p -type conduction mechanism at the same time. Meanwhile, an n -type 2D ReS₂ multilayers has
3 been suggested as a promising candidate for optoelectronic applications, mainly because of its
4 thickness-independent all direct bandgap and decoupled vdW interaction. The larger interlayer
5 resistance of ReS₂ compared to that of other vdW materials such as MoS₂ and graphene
6 facilitates the conducting channel migration under electrostatic bias conditions [23].

7 In this work, we reveal the presence of a top-surface channel hindering from undesired
8 ambient adsorbates and surface oxides in a multilayer p -type black phosphorus (BP) and n -
9 type rhenium disulfide (ReS₂) as representative materials. The surface adsorbates and oxides
10 not only reduce the electron density ($1.26 \times 10^{12} \text{ cm}^{-2} \sim 2.88 \times 10^{12} \text{ cm}^{-2}$ in ReS₂ multilayers)
11 but also suppress the field-effect mobility (about 27.6 % for holes in BP and 26.3 % for
12 electrons in ReS₂ multilayers at $V_D = 5 \text{ V}$), prohibiting the presence of second hump in a
13 transconductance (g_m) under ambient conditions. In particular, the field-effect mobility of ReS₂
14 increases with drain bias (V_D) at a high vacuum condition, meanwhile this mobility decreases
15 with V_D at ambient conditions. This contradictory carrier mobility reliance on V_D further
16 supports the restricted formation of conducting top-surface channel and limited spatial channel
17 migration along the thickness. We confirmed additionally the negligible variation in drain bias
18 polarity-dependent turn-on voltage for the bottom-channel of ReS₂ multilayer under ambient
19 conditions, supporting an exclusive contribution of surface adsorbates to the formation of top-
20 channel in 2D multilayers.

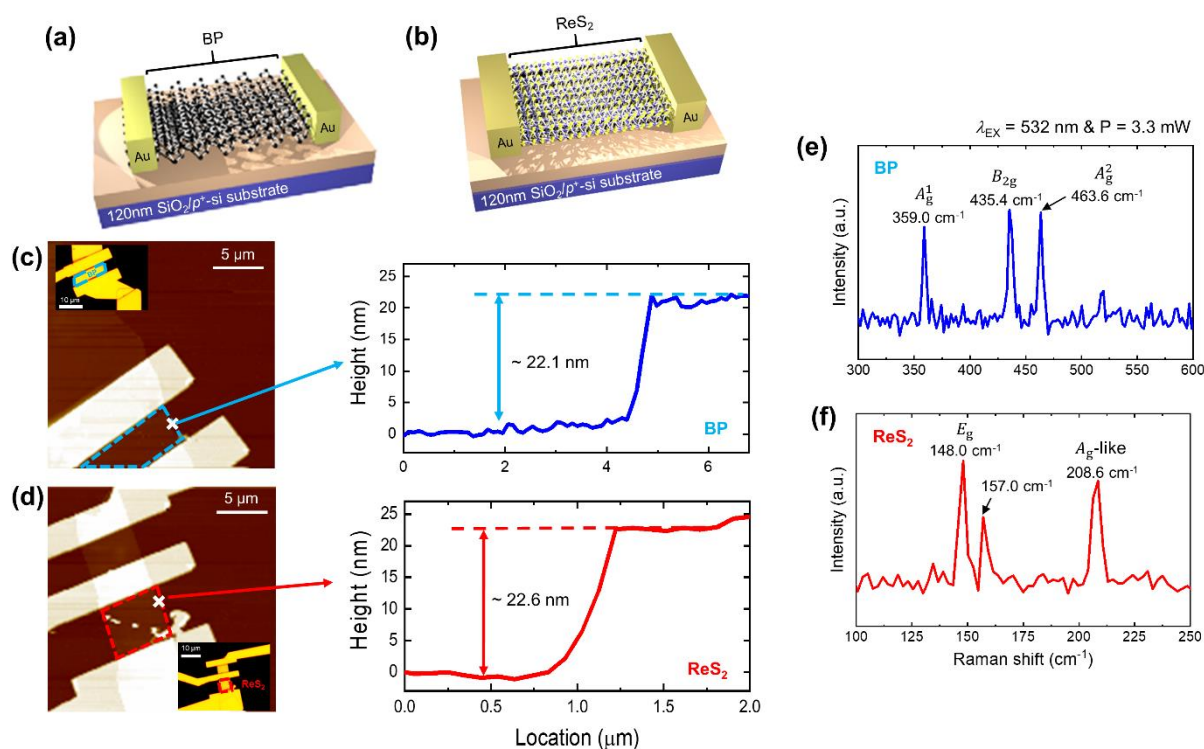
21 **2. Materials and device fabrications**

1 For this study, we fabricated 2D multilayer BP and ReS₂ transistors using a conventional dry
2 transfer method [24,25] as illustrated in Figures 1a-b. The properly chosen mechanically
3 exfoliated BP and ReS₂ flakes were first placed on a 120 nm SiO₂/p⁺-Si substrate. To define
4 active channel area using metal electrodes, a bilayer poly (methyl methacrylate) (PMMA: EL11
5 and C4) was spread evenly on multilayer flakes by spin-coater and selective electron-beam
6 lithography (Elphy Quantum, Raith) was performed. Au (280 nm) metal deposition was carried
7 out using an electron-beam evaporator after the development of PMMA. The optical images of
8 the fabricated BP and ReS₂ devices are displayed in Figures 1c-d, respectively (Eclipse LV
9 150N, Nikon). The thicknesses of the multilayer BP (≈ 22.1 nm) and ReS₂ (≈ 22.6 nm) were
10 confirmed via atomic force microscopy (AFM, Park Systems, NX10) under ambient conditions.
11 The channel length and width ratios were also confirmed ($L/W = 4.5 \mu\text{m}/13.2 \mu\text{m}$ for BP and
12 $= 5.5 \mu\text{m}/5.5 \mu\text{m}$ for ReS₂).

13 The fabricated devices were thermally annealed in two steps, that is, i) for 9 h at 423 K and
14 ii) for 1 h at 656 K, under a high-vacuum condition ($< 10^{-6}$ Torr) to obtain a clean surface and
15 low metal-to-semiconductor Schottky barrier. Notably, the multilayer devices were placed in a
16 high-vacuum chamber for one month before the electrical characterization to exclude
17 unnecessarily physisorbed surface adsorbates on the top surface of the materials. The
18 effectiveness of our thermal treatment under the high-vacuum condition is discussed further in
19 supporting information (see Figure S1). In addition, to ensure the formation of adsorbates on
20 the surface of 2D materials in addition to surface oxidation, all electrical characterizations
21 (B1500A, Keysight) under ambient conditions were conducted within a day after 1.5 h of air
22 venting. Figures 1e-f present the optical Raman spectra (XperRAM C series, Nanobase)
23 measured from the BP and ReS₂ flakes with a laser excitation wavelength (λ_{EX}) of 532 nm at a

1 power of 3.3 mW, respectively. The observed dominant vibration modes of A_g^1 (≈ 359.0 cm^{-1}),
 2 A_g^2 (≈ 463.6 cm^{-1}), and B_{2g} (≈ 435.4 cm^{-1}) peaks indicate the multilayer BP, whereas the
 3 obtained E_g (≈ 150 – 160 cm^{-1}) and A_g -like (≈ 208.6 cm^{-1}) peaks indicate the multilayer ReS₂.
 4 The characteristic frequencies for both flakes were consistent with those in previous reports
 5 [20,23,26,27].

6



7

8 **Figure 1.** Device structure and optical Raman spectra of multilayer TMDs. Device schematics
 9 of multilayer (a) BP and (b) ReS₂ transistors. AFM images of our (c) BP and (d) ReS₂ devices
 10 to confirm the thickness profile with 5 μm scale bar. The corresponding optical images with
 11 10 μm scale bar are presented in the inset. Representative Raman spectra for the (e) BP and (f)
 12 ReS₂ multilayers.

13

14

3. Results and discussion

3.1 Electrical properties of *p*-type BP multilayers

The V_D -dependent drain current (I_D) output characteristic curves of the multilayer BP under high-vacuum and ambient conditions are directly compared for representative back-gate bias (V_G) values ranging from -10 V to -40 V in steps of -10 V, as displayed in Figure 2a. The observed pseudolinear tendency indicates an ohmic-like contact property at the Au–ReS₂ interface regardless of the case, demonstrating the effectiveness of our two-step annealing process. In addition, the measured I_D under ambient conditions was less than that under high-vacuum conditions. We attributed this suppression of conductance to the effects of numerous Coulomb impurities on top of the BP in addition to surface oxidation, which modifies the carrier density profile along the thickness of the BP.

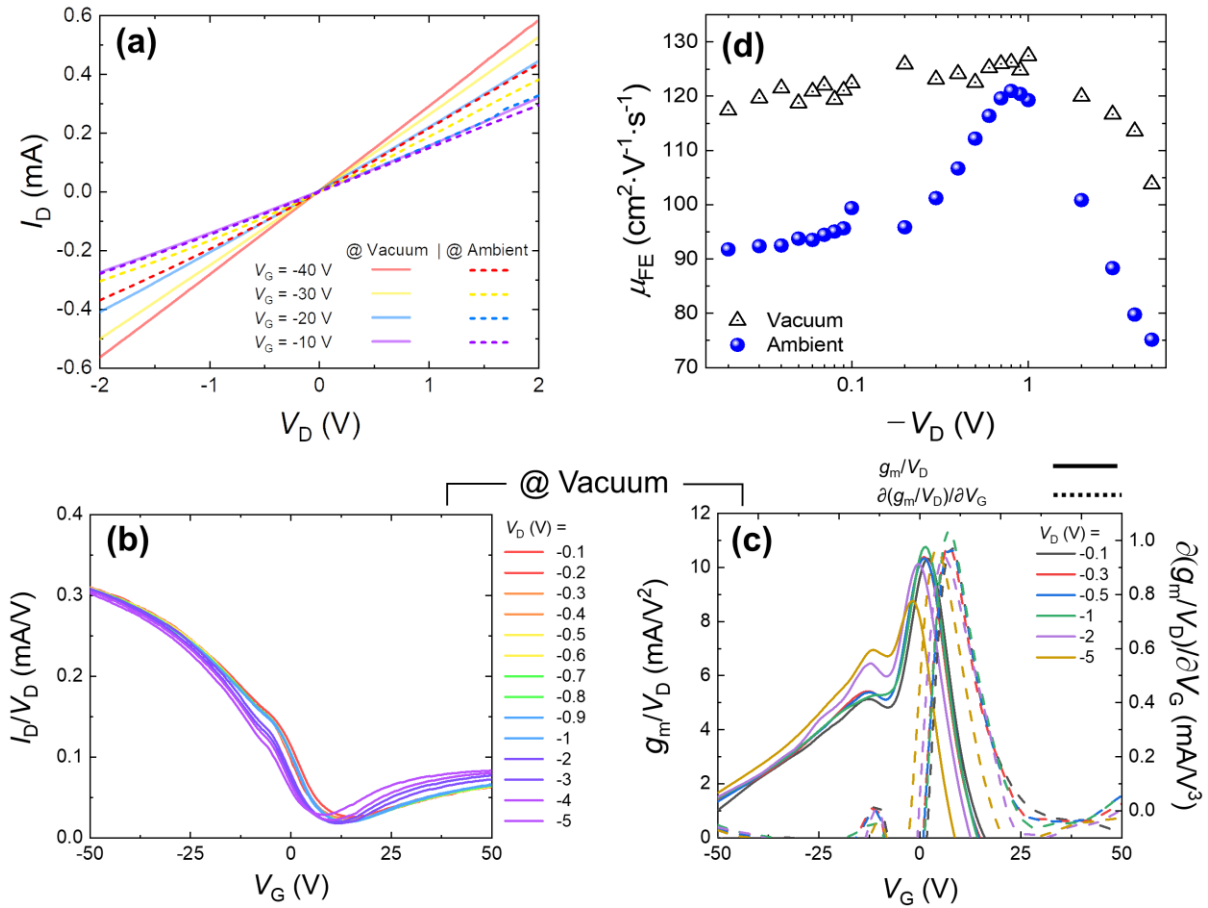
Previous theoretical and experimental studies have revealed that the V_D - and/or V_G -dependent interlayer resistance or energy barrier enables the modification of the carrier density profile along the *c*-axis of 2D multilayers [28,29]. This results in the presence of two plateaus in their transconductance ($g_m = (\partial I_D / \partial V_G)$) and derivative of g_m ($dg_m = \partial g_m / \partial V_G$) curves after V_D normalization with a single gate configuration [23]. To explore the effects of surface adsorbates including surface oxidation on the carrier transport system in 2D multilayer BP, the V_D -normalized V_G -dependent I_D transfer curves (I_D / V_D) for a high-vacuum condition are displayed in Figure 2b. The enhancement of I_D with decreasing V_G indicates *p*-type carrier transport in the BP transistor. The corresponding g_m and dg_m curves are shown in Figure 2c. In this figure, two humps can be observed, and they merge with increasing $|V_D|$ at high V_D conditions ($|V_D| > 1$ V), manifesting the shift of most conducting channel from the bottom to the top surface driven by reduced interlayer resistance regardless of V_D (see Figure S2) [28,30]. In addition, the two-

1 peak of dg_m is exhibited at almost the same V_G values at all given V_D , indicating a multichannel
2 carrier transport in the BP device (see Figures S3a-b). Meanwhile, under ambient conditions,
3 the second peak of dg_m gradually disappears at high V_D ($|V_D| > 1$ V), as shown in Figures S3c-
4 d. This anomalous feature indicates the disappearance of the top channel in the BP multilayers
5 owing to undesired adsorbates on the surface under ambient conditions in addition to surface
6 oxidation. The two unexpected peaks in the relatively low V_D regime ($V_D < 1$ V) under ambient
7 conditions appear to be mainly due to the high contact resistance caused by adsorbate invasion
8 into the Au–BP interface (see Figure S4) [31].

9 We also examined the V_D -dependent field-effect mobility ($\mu_{FE} = g_m \cdot (L/W) \cdot C_{OX}^{-1} \cdot V_D^{-1}$, where
10 C_{OX} denotes the oxide planar capacitance per unit area) for both conditions (Figure 2d), to
11 discuss the carrier scattering effects arising from surface adsorbates. The μ_{FE} increases with
12 $|V_D|$ up to 1 V and drops abruptly at $|V_D| > 1$ V for both cases. We ascribed the enhancement of
13 μ_{FE} to the reduction of the interlayer resistance with increasing $|V_D|$. Meanwhile, the observed
14 dramatic suppression of μ_{FE} in the high V_D regime, which is closely associated with the
15 cleanliness of the top channel, can be attributed to the undesired adsorbate effects in addition
16 to surface oxidation, hiding the formation of the top-surface channel. As expected, the μ_{FE} of
17 BP under ambient conditions declines more rapidly than that under high-vacuum conditions,
18 demonstrating the effects of surface adsorbates and surface oxidation on the carrier mobility
19 and/or contact resistance [11]. Furthermore, the higher values of μ_{FE} under high-vacuum
20 conditions than those under ambient conditions, regardless of V_D , support the scenario that
21 carrier scattering from impurities resulted in mobility suppression, particularly on the top
22 surface. Despite the different features between high-vacuum and ambient conditions, the
23 instability of BP causing the inevitable degradation of the device hampers the apparent

1 manifestation of the importance of the cleanliness of the top channel for its formation, requiring
 2 additional evaluation with other 2D materials.

3



4

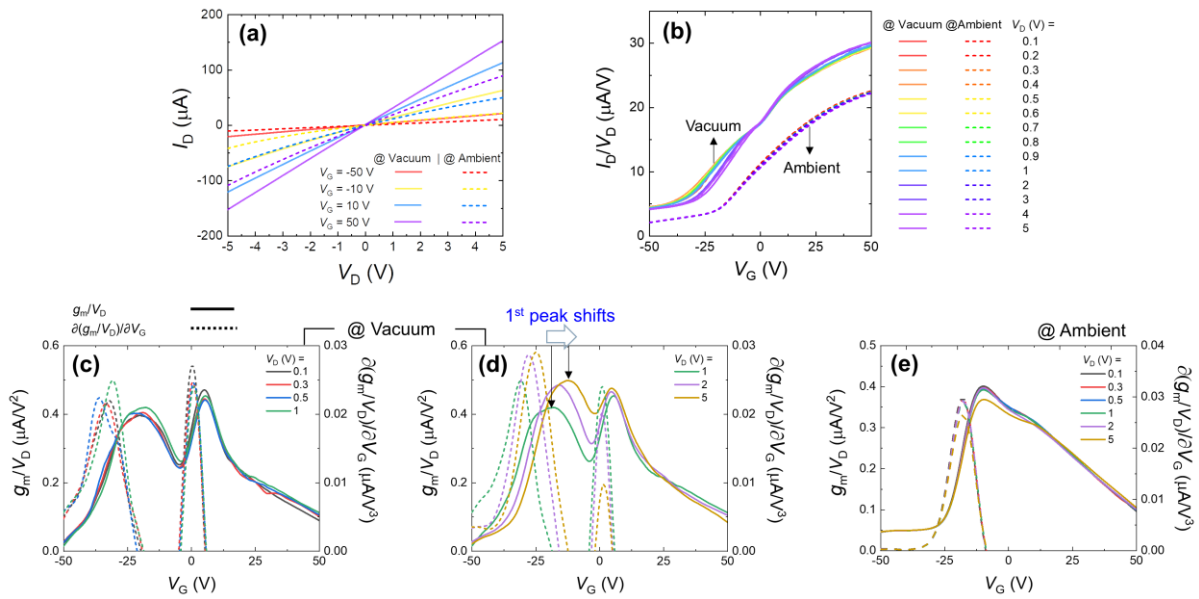
5 **Figure 2.** Electrical characterization of the *p*-type BP multilayers. (a) I_D – V_D output
 6 characteristic curve comparison at high-vacuum and ambient conditions. V_D -normalized (b)
 7 I_D – V_G transfer curves, (c) $g_m = ((\partial I_D/\partial V_G)/V_D)$ curves, and $dg_m (= \partial g_m/\partial V_G)$ curves at the high-
 8 vacuum condition, respectively. (d) V_D -dependent μ_{FE} for both high-vacuum and ambient
 9 conditions.

10

11

1 3.2 Electrical properties of *n*-type ReS₂ multilayers

2 We performed similar measurements (e.g., output characteristic curves, transfer curves, the
 3 corresponding g_m and dg_m curves, field-effect mobility, and turn-on voltage (V_T)) on the *n*-type
 4 ReS₂ multilayers to demonstrate the similar distinctive carrier transport as in the *p*-type BP
 5 counterparts. The V_D -dependent output characteristic curves show a high linearity of the
 6 multilayer ReS₂ under both high-vacuum and ambient conditions (Figure 3a), indicating the
 7 negligible Schottky barrier effects in the observed V_G regime. In addition, the measured I_D
 8 under high-vacuum conditions is superior to that measured under ambient conditions, which is
 9 consistent with the aforementioned BP behavior, manifesting Coulomb impurity effects on the
 10 top channel of 2D materials under ambient conditions.



11

12 **Figure 3.** Electrical characterization of the *n*-type ReS₂ multilayers. (a) I_D - V_D output
 13 characteristics at high-vacuum and ambient conditions. V_D -normalized (b) I_D - V_G transfer
 14 curves, and (c) g_m and dg_m curves at the high-vacuum condition for the low V_D and (d) high V_D
 15 regimes. (e) V_D -normalized g_m and dg_m curves at the ambient condition.

16

1 The V_G -dependent I_D transfer curves normalized by V_D (I_D/V_D) are presented in Figure 3b for
2 both conditions. The observed enhancement of I_D with increasing V_G at the given V_D values
3 indicates a typical n -type behavior. As mentioned in the previous section, the two plateaus of
4 g_m indicate different carrier densities along the c -axis in 2D multilayer devices, indicating both
5 bottom- and top-channel formation. In Figures 3b-3d, we can observe these distinct features in
6 the multilayer ReS₂ device under high-vacuum conditions. In these figures, we can observe the
7 shape change of V_D -dependent conductance and the anomalous humps exclusively under high-
8 vacuum conditions, which is in contrast to that under ambient conditions. In addition, as V_D
9 increases, the two peaks of g_m gradually extend and merge (see Figure 3d), indicating channel
10 migration from the bottom to the top surface driven by reduced interlayer resistance [20]. As
11 this anomalous signature reveals not only conduction channel migration but also the important
12 role of surface cleanliness for the formation of top-surface channels in 2D multilayers, the
13 absence of a second peak in the g_m and dg_m curves under ambient conditions indicates the
14 vanished top-surface channel inside the 2D multilayers (see Figure 3e). Furthermore, the
15 observed almost-identical V_D -normalized g_m curves regardless of the conditions demonstrate a
16 negligible Au-metal-to-ReS₂ Schottky barrier effect, particularly for small V_D regimes ($V_D < 1$
17 V) (see Figures 3c-e).

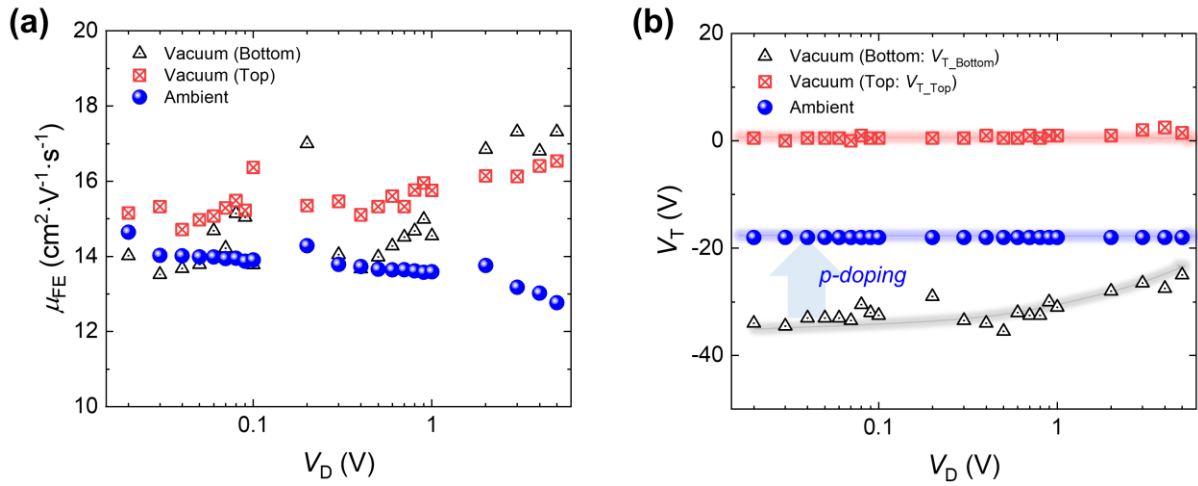


Figure 4. (a) V_D -dependent μ_{FE} and (b) V_T of our ReS₂ devices at high-vacuum and ambient conditions.

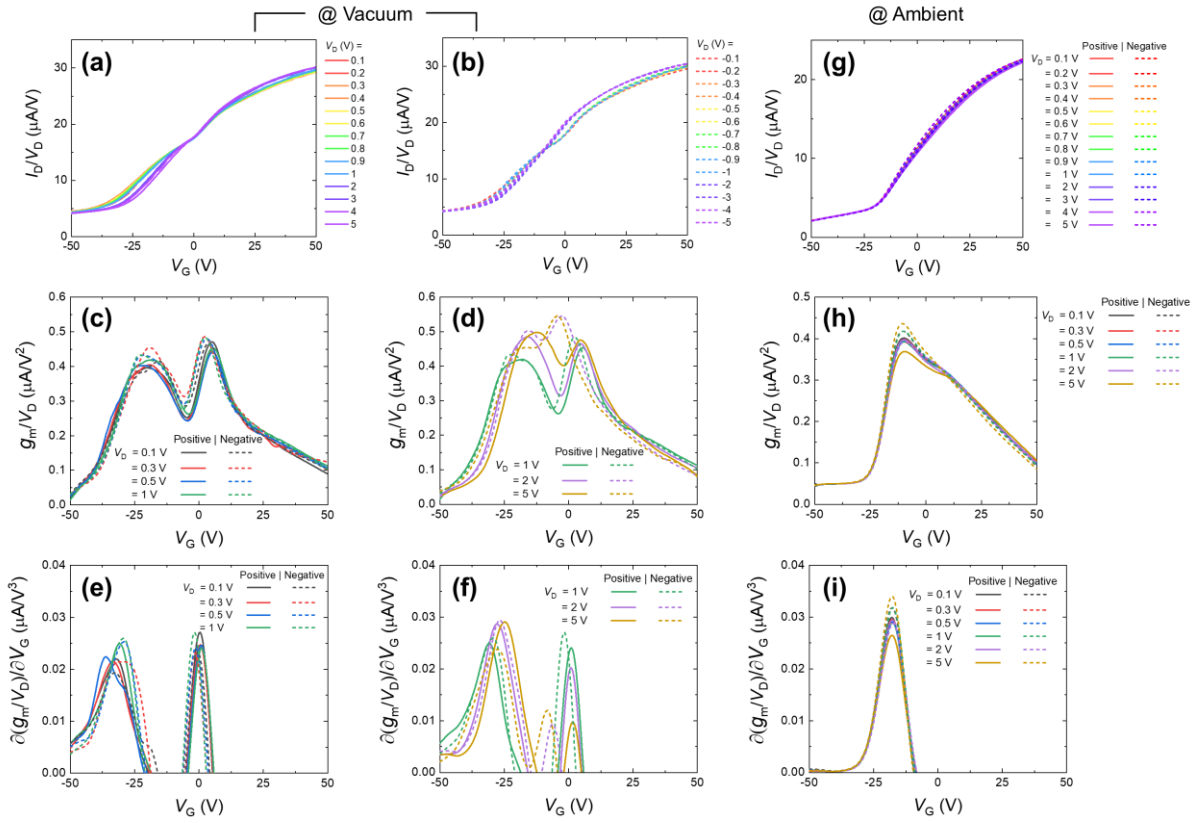
Subsequently, we investigated the V_D -dependent μ_{FE} in both conditions to confirm the important role of top-surface cleanliness in top-channel formation in 2D multilayers. As the increment of V_D reduces the effect of interlayer resistance in addition to the conduction channel migration, the determined maximum μ_{FE} increases with increasing V_D in terms of the total conductance of the device, as displayed in Figure 4a. Meanwhile, the μ_{FE} obtained under ambient conditions decreases with V_D , again suggesting the substantial effect of Coulomb impurities on the top of ReS₂, which interferes with the channel migration. The μ_{FE} suppression in ReS₂ devices exclusively under ambient conditions, which is consistent with the aforementioned μ_{FE} tendency in BP in the high V_D regime ($|V_D| > 1$ V), restricts carrier transport properties owing to the unclean surface. Moreover, these impurities induce an undesired surface *p*-doping effect on the top of ReS₂, not only leading to the shift of V_T positively but also masking the formation of the top-surface channel inside the 2D multilayers (see Figure 4b). In particular, the observation of i) almost constant V_T values for the top-channel ($V_{T_Top} \approx$

1 0.5 V) regardless of V_D and ii) increasing V_T values for the bottom channel ($V_{T_Bottom} = -34$ V–
 2 -25 V) with increasing V_D indicating the bottom-channel migration to achieve a minimum
 3 resistive path inside the ReS₂ multilayers under the high-vacuum condition. However, the
 4 obtained V_D -dependent $V_{T_ambient}$ (≈ -18.5 V) under ambient conditions is almost pinned,
 5 indicating that the restricted channel migration is mainly driven by the numerous surface
 6 adsorbates on the top of ReS₂, overwhelming the advantages of the channel migration and
 7 reduced interlayer resistance in the ReS₂ multilayers. The electron density is suppressed by \approx
 8 $1.26 \times 10^{12} \text{ cm}^{-2}$ – $2.88 \times 10^{12} \text{ cm}^{-2}$ ($= C_{OX}/q \times (\Delta V_T)$, where q denotes the electronic unit charge)
 9 and μ_{FE} is decreased to ≈ 26.3 % at $V_D = 5$ V in ReS₂.

10 *3.3 Drain bias polarity effects on carrier transport in 2D multilayers*

11 In addition, we present the I_D , g_m , and dg_m curves as a function of the polarity of V_D for both
 12 conditions to clarify the formation of the top surface in 2D multilayers. Indeed, when an
 13 insignificant Schottky barrier effect exhibits on the channel migration, there is a negligible
 14 difference among them regardless of the conditions. Figures 5a-f demonstrate the I_D/V_D , g_m/V_D ,
 15 and dg_m/V_D curves for positive and negative V_D , respectively, under high-vacuum conditions.
 16 In these figures, most of the curves are almost identical when V_D is less than ± 1 V. However,
 17 as V_D decreases further, the g_m/V_D curve broadens and merges faster than when V_D is positive
 18 (see Figure 5d), which is observed in the corresponding dg_m/V_D curves (see Figure 5f). We
 19 ascribed this quick channel migration to a strong effective gate-to-drain electrostatic bias (V_{G-}
 20 $D = V_G - V_D$) condition, enhancing consequently the channel migration with the suppressed
 21 interlayer resistance. It should be underlined that when V_D is negative, V_{G-D} is always higher
 22 than that when V_D is positive. In addition, the V_G position corresponding to the second
 23 maximum dg_m/V_D shifts negatively when V_D is negative, which indicates the spatial

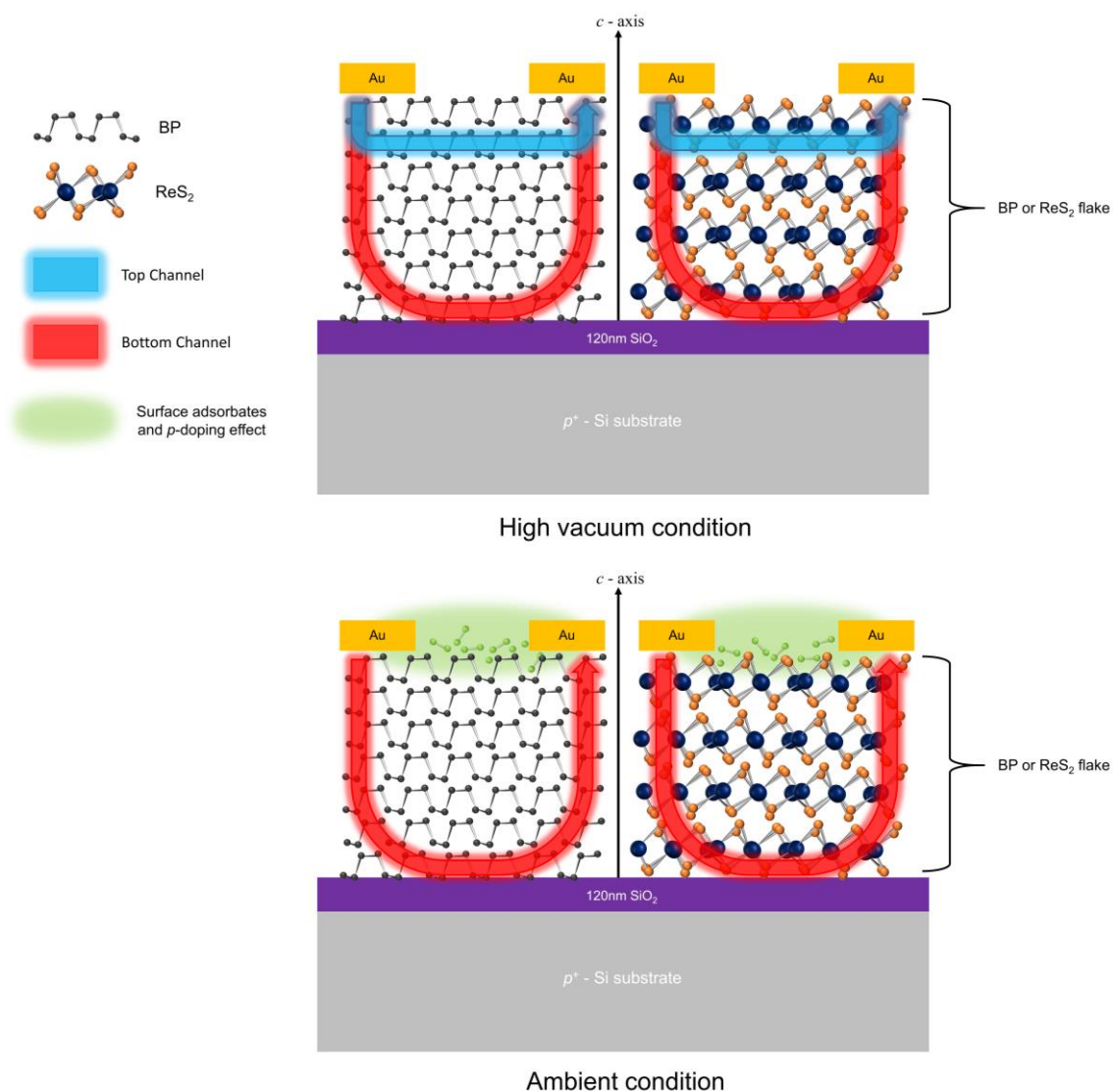
1 modification of the conducting channel, and more importantly, results in an enhanced carrier
2 mobility. Meanwhile, the observed I_D/V_D , g_m/V_D , and dg_m/V_D curves under ambient conditions
3 are similar to each other regardless of the polarity of V_D , demonstrating the considerable
4 adsorbate effects on the top of ReS_2 on the formation of the top channel in the 2D multilayers
5 (see Figures 5g-i). More specifically, when surface adsorbates causing an undesired p -doping
6 effect are placed onto the surface of n -type multilayer ReS_2 , the Fermi level of the top channel
7 would be down-shifted, limiting the large modulation of R_{Int} under electrostatic V_D/V_G bias
8 conditions. Consequently, the top channel formation and channel migration would be strongly
9 restricted as demonstrated in Figures 5g-i under ambient conditions. To observe the surface
10 adsorbate effects on 2D multilayers, the presence (or not) of top channel with regards to the
11 conditions (ambient or high vacuum) is demonstrated by presenting a conceptual illustration of
12 the vanished top-surface channel under ambient conditions, as shown in Figure 6. Additionally,
13 we confirmed another ReS_2 channel locating the upper part on the same ReS_2 flake,
14 demonstrating consistent results (see Figure 1d and S5).



1

2 **Figure 5.** V_D polarity effects on the carrier transport mechanism. V_D -normalized (a-b) I_D - V_G
 3 transfer curves, (c-d) g_m curves, and (e-f) dg_m curves for the high-vacuum condition. Sample
 4 plots for the ambient condition; (g) I_D - V_G transfer curves, (h) g_m curves, and (i) dg_m curves.

5



1

2 **Figure 6.** Conceptual illustration of the vanished top-channel in BP and ReS₂ due to surface
 3 adsorbate effects

4

5 **4. Conclusions**

6 We report the surface effect of 2D devices in terms of Coulomb impurities, such as atomic
 7 defects, oxide fixed charges, impurities, chemical residues, surface oxides and undesired
 8 surface adsorbates, including oxygen and water molecules. Identical electrical

1 characterizations were conducted under both high-vacuum and ambient conditions on BP and
2 ReS₂ devices to elucidate the conductivity reduction due to undesired surface adsorbates. It
3 was observed that the charge density was reduced and the mobility decreased under ambient
4 conditions. We attribute these electrical performance degradations to the disappearance (or
5 decline) of the top channel due to undesired Coulomb scatters and the *p*-doping effect on the
6 top surfaces in addition to surface oxidation. Our findings can provide a better understanding
7 of distinct carrier transport features in addition to the importance of top surface cleanliness, not
8 only for BP and ReS₂, but also for all types of 2D multilayered devices.

9 **Data availability statement**

10 The data that support the findings of this study are available upon reasonable request from the
11 authors.

12 **Acknowledgments**

13 This study was supported by a National Research Foundation of Korea (NRF) grant funded
14 by the Korean government (MSIT) (NRF-2019R1C1C1003467 & NRF-2022R1A2C4001245)
15 and by Sookmyung Women's University Research Grants (1-0000-0000).

16 **Conflicts of interest**

17 The authors declare no conflicts of interest.

18 **Supplementary information**

19 Figure S1. (a) Optical image of 10 nm-thick multilayer BP multilayers. (b) Semi-logarithmic
20 scaled transfer characteristic curves (I_D - V_G) at $V_D = 1.0$ V after the thermal annealing process
21 at high-vacuum condition with a different sweep direction. (c) V_D -dependent transfer curves.

1 Figure S2. (a) Measurement schematic to obtain interlayer resistance (R_{Int}) of ReS₂ multilayers
2 via c-AFM. (b) Current-voltage characteristics at Au substrate. (c) Determined R_{Int} of ReS₂
3 multilayer as a function of voltage.

4 Figure S3. V_{D} -normalized derivative of transconductance under (a) high vacuum and (b)
5 ambient conditions.

6 Figure S4. 3D illustrations presenting surface adsorbates effects on both channel and contact
7 property.

8 Figure S5. (a) AFM image of the confirmed ReS₂ device locating the upper part on the same
9 ReS₂ flake. V_{D} -normalized (b) $I_{\text{D}}-V_{\text{G}}$ transfer curves, and (c) $g_{\text{m}} = ((\partial I_{\text{D}}/\partial V_{\text{G}})/V_{\text{D}})$ curves at the
10 high-vacuum and ambient conditions, respectively.

11

1 **References**

- 2 [1] Moon B H, Bae J J, Joo M-K, Choi H, Han G H, Lim H and Lee Y H 2018 Soft
3 Coulomb gap and asymmetric scaling towards metal-insulator quantum criticality in
4 multilayer MoS₂ *Nat. Commun.* **9** 2052
- 5 [2] Jin Y, Joo M-K, Moon B H, Kim H, Lee S, Jeong H Y and Lee Y H 2020 Coulomb
6 drag transistor using a graphene and MoS₂ heterostructure *Commun. Phys.* **3** 189
- 7 [3] Calman E V, Fogler M M, Butov L V, Hu S, Mishchenko A and Geim A K 2018
8 Indirect excitons in van der Waals heterostructures at room temperature *Nat. Commun.*
9 **9** 1895
- 10 [4] Liu H, Chen J, Yu H, Yang F, Jiao L, Liu G-B, Ho W, Gao C, Jia J, Yao W and Xie M
11 2015 Observation of intervalley quantum interference in epitaxial monolayer tungsten
12 diselenide *Nat. Commun.* **6** 8180
- 13 [5] Zhang Y, Tan Y-W, Stormer H L and Kim P 2005 Experimental observation of the
14 quantum Hall effect and Berry's phase in graphene *Nature* **438** 201–4
- 15 [6] Song S H, Joo M-K, Neumann M, Kim H and Lee Y H 2017 Probing defect dynamics
16 in monolayer MoS₂ via noise nanospectroscopy *Nat. Commun.* **8** 2121
- 17 [7] Sim D M, Kim M, Yim S, Choi M-J, Choi J, Yoo S and Jung Y S 2015 Controlled
18 Doping of Vacancy-Containing Few-Layer MoS₂ via Highly Stable Thiol-Based
19 Molecular Chemisorption *ACS Nano* **9** 12115–23
- 20 [8] Namgung S D, Yang S, Park K, Cho A-J, Kim H and Kwon J-Y 2015 Influence of post-
21 annealing on the off current of MoS₂ field-effect transistors *Nanoscale Res. Lett.* **10** 62
- 22 [9] Bolshakov P, Smyth C M, Khosravi A, Zhao P, Hurley P K, Hinkle C L, Wallace R M
23 and Young C D 2019 Contact Engineering for Dual-Gate MoS₂ Transistors Using O₂
24 Plasma Exposure *ACS Appl. Electron. Mater.* **1** 210–9
- 25 [10] Liu Y S, Yang X F, Hong X K, Si M S, Chi F and Guo Y 2013 A high-efficiency double
26 quantum dot heat engine *Appl. Phys. Lett.* **103** 093901
- 27 [11] Joo M-K, Yun Y, Ji H and Suh D 2019 Coulomb scattering mechanism transition in
28 2D layered MoTe₂: effect of high- κ passivation and Schottky barrier height
29 *Nanotechnology* **30** 035206
- 30 [12] Liu H, Han N and Zhao J 2015 Atomistic insight into the oxidation of monolayer
31 transition metal dichalcogenides: from structures to electronic properties *RSC Adv.* **5**
32 17572–81
- 33 [13] Cui X, Lee G-H, Kim Y D, Arefe G, Huang P Y, Lee C-H, Chenet D A, Zhang X,
34 Wang L, Ye F, Pizzocchero F, Jessen B S, Watanabe K, Taniguchi T, Muller D A, Low
35 T, Kim P and Hone J 2015 Multi-terminal transport measurements of MoS₂ using a van
36 der Waals heterostructure device platform *Nat. Nanotechnol.* **10** 534–40
- 37 [14] Li S-L, Wakabayashi K, Xu Y, Nakaharai S, Komatsu K, Li W-W, Lin Y-F, Aparecido-
38 Ferreira A and Tsukagoshi K 2013 Thickness-Dependent Interfacial Coulomb
39 Scattering in Atomically Thin Field-Effect Transistors *Nano Lett.* **13** 3546–52
- 40 [15] Chang P, Liu X, Liu F and Du G 2019 First-principles based ballistic transport
41 simulation of monolayer and few-layer InSe FETs *Jpn. J. Appl. Phys.* **58**
- 42 [16] Das S and Appenzeller J 2013 Screening and interlayer coupling in multilayer MoS₂
43 *Phys. status solidi - Rapid Res. Lett.* **7** 268–73
- 44 [17] Lembke D, Allain A and Kis A 2015 Thickness-dependent mobility in two-dimensional
45 MoS₂ transistors *Nanoscale* **7** 6255–60

- 1 [18] Choi W, Choudhary N, Han G H, Park J, Akinwande D and Lee Y H 2017 Recent
2 development of two-dimensional transition metal dichalcogenides and their applications
3 *Mater. Today* **20** 116–30
- 4 [19] Das S and Appenzeller J 2013 Where Does the Current Flow in Two-Dimensional
5 Layered Systems? *Nano Lett.* **13** 3396–402
- 6 [20] Kim S Y, Jeong D, Lee H, Na I, Kim S, Kim D, Lim S, Lee B C, Lee S, Yang S M,
7 Kim G-T and Joo M-K 2020 Drain induced barrier increasing in multilayer ReS₂ *2D*
8 *Mater.* **7** 031004
- 9 [21] Buscema M, Island J O, Groenendijk D J, Blanter S I, Steele G A, van der Zant H S J
10 and Castellanos-Gomez A 2015 Photocurrent generation with two-dimensional van der
11 Waals semiconductors *Chem. Soc. Rev.* **44** 3691–718
- 12 [22] Moon Y-S, Shon J H, Kim D, Lee K, Joo M-K and Kim G-T 2020 Understanding
13 tunable photoresponsivity of two-dimensional multilayer phototransistors: Interplay
14 between thickness and carrier mobility *Appl. Phys. Lett.* **116** 183102
- 15 [23] Lee B C, Na J, Choi J H, Ji H, Kim G-T and Joo M-K 2018 Probing Distinctive Electron
16 Conduction in Multilayer Rhenium Disulfide *Adv. Mater.* **31** 1805860
- 17 [24] Novoselov K S 2004 Electric Field Effect in Atomically Thin Carbon Films *Science*
18 *(80-.)*. **306** 666–9
- 19 [25] Novoselov K S, Jiang D, Schedin F, Booth T J, Khotkevich V V, Morozov S V and
20 Geim A K 2005 Two-Dimensional Atomic Crystals *Proc. Natl. Acad. Sci. U. S. A.* **102**
21 10451
- 22 [26] Tongay S, Sahin H, Ko C, Luce A, Fan W, Liu K, Zhou J, Huang Y-S, Ho C-H, Yan J,
23 Ogletree D F, Aloni S, Ji J, Li S, Li J, Peeters F M and Wu J 2014 Monolayer behaviour
24 in bulk ReS₂ due to electronic and vibrational decoupling. *Nat. Commun.* **5** 3252
- 25 [27] Xu K, Deng H-X, Wang Z, Huang Y, Wang F, Li S-S, Luo J-W and He J 2015 Sulfur
26 vacancy activated field effect transistors based on ReS₂ nanosheets *Nanoscale* **7** 15757–
27 62
- 28 [28] Kim C, Sung M, Kim S Y, Lee B C, Kim Y, Kim D, Kim Y, Seo Y, Theodorou C, Kim
29 G-T and Joo M-K 2021 Restricted Channel Migration in 2D Multilayer ReS₂ *ACS Appl.*
30 *Mater. Interfaces* **13** 19016–22
- 31 [29] Lee B C, Kim C M, Kim S, Kim G-T and Joo M-K 2020 Effect of interlayer tunneling
32 barrier on carrier transport and fluctuation in multilayer ReS₂ *Appl. Phys. Lett.* **117**
33 033501
- 34 [30] Tavkhelidze A, Bibilashvili A, Jangidze L and Gorji N E 2021 Fermi-Level Tuning of
35 G-Doped Layers *Nanomaterials* **11** 505
- 36 [31] Lee B C, Kim C M, Jang H, Lee J W, Joo M-K and Kim G-T 2017 Degradation pattern
37 of black phosphorus multilayer field-effect transistors in ambient conditions: Strategy
38 for contact resistance engineering in BP transistors *Appl. Surf. Sci.* **419** 637–41
39